

Planckian dissipation and scale invariance in a quantum-critical disordered pnictide

Yasuyuki Nakajima,^{1,2} Tristin Metz,² Christopher Eckberg,² Kevin Kirshenbaum,² Alex Hughes,² Renxiong Wang,² Limin Wang,² Shanta R. Saha,² I-Lin Liu,^{2,3,4} Nicholas P. Butch,^{2,4} Daniel Campbell,² Yun Suk Eo,² David Graf,⁵ Zhonghao Liu,^{6,7} Sergey V. Borisenko,⁶ Peter Y. Zavalij,⁸ and Johnpierre Paglione^{2,9}

¹*Department of Physics, University of Central Florida, Orlando, Florida 32816*

²*Center for Nanophysics and Advanced Materials, Department of Physics, University of Maryland, College Park, Maryland 20742*

³*Chemical Physics Department, University of Maryland, College Park, Maryland 20742*

⁴*NIST Center for Neutron Research, National Institute of Standards and Technology, Gaithersburg, Maryland 20899*

⁵*National High Magnetic Field Laboratory, Florida State University, Tallahassee, Florida 32310*

⁶*IFW-Dresden, Helmholtzstraße 20, 01171 Dresden, Germany*

⁷*Shanghai Institute of Microsystem and Information Technology, Chinese Academy of Sciences, Shanghai 200050, China*

⁸*Department of Chemistry, University of Maryland, College Park, Maryland 20742*

⁹*The Canadian Institute for Advanced Research, Toronto, ON M5G 1Z8, Canada*

(Dated: February 28, 2019)

Quantum-mechanical fluctuations between competing phases at $T = 0$ induce exotic finite-temperature collective excitations that are not described by the standard Landau Fermi liquid framework [1–4]. These excitations exhibit anomalous temperature dependences, or non-Fermi liquid behavior, in the transport and thermodynamic properties [5] in the vicinity of a quantum critical point, and are often intimately linked to the appearance of unconventional Cooper pairing as observed in strongly correlated systems including the high- T_c cuprate and iron pnictide superconductors [6, 7]. The presence of superconductivity, however, precludes direct access to the quantum critical point, and makes it difficult to assess the role of quantum-critical fluctuations in shaping anomalous finite-temperature physical properties, such as Planckian dissipation $\hbar/\tau_p = k_B T$ [8–10]. Here we report temperature-field scale invariance of non-Fermi liquid thermodynamic, transport and Hall quantities in a non-superconducting iron-pnictide, $\text{Ba}(\text{Fe}_{1/3}\text{Co}_{1/3}\text{Ni}_{1/3})_2\text{As}_2$, indicative of quantum criticality at zero temperature and zero applied magnetic field. Beyond a linear in temperature resistivity, the hallmark signature of strong quasiparticle scattering, we find a more universal Planck-limited scattering rate that obeys a scaling relation between temperature and applied magnetic fields down to the lowest energy scales. Together with the emergence of hole-like carriers close to the zero-temperature and zero-field limit, the scale invariance, isotropic field response and lack of applied pressure sensitivity point to the realization of a novel quantum fluid predicted by the holographic correspondence [11–13] and born out of a unique quantum critical system that does not drive a pairing instability.

PACS numbers:

Non-Fermi liquid (NFL) behavior ubiquitously appears in iron-based high-temperature superconductors with a novel type of superconducting pairing symmetry driven by interband repulsion [7, 14]. The putative pairing mechanism is thought to be associated with the temperature-doping phase diagram, bearing striking resemblance to cuprate and heavy-fermion superconductors [15, 16]. In iron-based superconductors, the superconducting phase appears to be centered around the point of suppression of antiferromagnetic (AFM) and orthorhombic structural order [14]. Close to the boundary between AFM order and superconductivity, the exotic metallic regime emerges in the normal state. In addition to the AFM order, the presence of an electronic nematic phase above the structural transition complicates the understanding of the SC and NFL behavior [17–20]. Moreover, the robust superconducting phase prohibits investigations of zero-temperature limit normal state physical properties associated with the quantum critical (QC) in-

stability due to the extremely high upper critical fields.

While AFM spin fluctuations are widely believed to provide the pairing glue in the iron-pnictides, other magnetic interactions are prevalent in closely related materials, such as the cobalt-based oxypnictides LaCoOX ($X=\text{P}, \text{As}$) [21], which exhibit ferromagnetic (FM) orders, and Co-based intermetallic arsenides with coexisting FM and AFM spin correlations [22–24]. For instance, a strongly enhanced Wilson ratio R_W of ~ 7 -10 at 2 K [25] and violation of the Koriga law [22–24] suggest proximity to a FM instability in BaCo_2As_2 . BaNi_2As_2 , on the other hand, seems to be devoid of magnetic order [26] and rather hosts other ordering instabilities in both structure and charge [27]. Confirmed by extensive study, Fe, Co, and Ni have the same 2+ oxidation state in the tetragonal ThCr_2Si_2 structure, thus adding one d electron- (hole-) contribution by Ni (Fe) substitution for Co in BaCo_2As_2 [28–31], and thereby modifying the electronic structure subtly but significantly enough to tune in

and out of different ground states and correlation types. Utilizing this balance, counter-doping a system to achieve the same nominal d electron count as BaCo_2As_2 can realize a unique route to the same nearly FM system while disrupting any specific spin correlation in the system.

Here, we utilize this approach to stabilize a novel ground state in the counter-doped non-superconducting iron pnictide $\text{Ba}(\text{Fe}_{1/3}\text{Co}_{1/3}\text{Ni}_{1/3})_2\text{As}_2$, also nearly ferromagnetic but with a unique type of spin fluctuation that leads to very strong quasiparticle scattering. We show that NFL behavior is prevalent in the very low temperature charge transport and thermodynamic properties of $\text{Ba}(\text{Fe}_{1/3}\text{Co}_{1/3}\text{Ni}_{1/3})_2\text{As}_2$, with temperature and magnetic energy scale invariance arising from a quantum critical ground state with fluctuation scattering limited by the Planckian dissipation bound, $\hbar/\tau_p = k_B T$. The hallmark of NFL behavior in $\text{Ba}(\text{Fe}_{1/3}\text{Co}_{1/3}\text{Ni}_{1/3})_2\text{As}_2$ is clearly observed in the resistivity (fig. 1a), which exhibits a quasi-linear T dependence over three orders of magnitude variation, from 20 K down to at least 20 mK at $B = 0$ T. In this temperature range, we find no discernible anomaly associated with phase transitions down to 20 mK, suggestive of the realization of an anomalous metallic ground state that persists to the $T = 0$ limit. Furthermore, this behavior is strongly suppressed with magnetic field, which drives a recovery of Fermi liquid (FL) behavior (i.e., $\rho \propto T^2$) at low temperatures (See Supplementary Material (SM)).

Mimicking the quasi-linear behavior in the temperature dependence of $\rho(T)$ at 0 T, the magnetoresistance (MR) at 1.31 K $\Delta R(B)/R(0)$ varies sublinearly with applied field up to 35 T (fig. 1b). The quasi-linear- T and B dependence allow us to introduce a new energy scale involving the scattering rate, the quadrature sum of temperature and magnetic field $\Gamma(T, B) \equiv \sqrt{(k_B T)^2 + (\eta \mu_B B)^2}$, where k_B is the Boltzmann constant, μ_B is the Bohr magneton, and η is a dimensionless parameter. Setting $\eta = 0.67$, we find the unusual scaling in the inelastic scattering rate $\hbar/\tau = \hbar m e^2 (\rho(T, B) - \rho(0, 0))/m^*$, where n is the carrier density and m^* is the effective mass, as a function of $\Gamma(T, B)$, collapsing onto one universal curve as shown in fig. 1c, reminiscent of the observation in QC iron-pnictide $\text{BaFe}_2(\text{As,P})_2$ [32].

The $\Gamma(T, B)$ scaling is closely correlated to the Planckian bound of dissipation. Quantum mechanics allows the shortest dissipative time scale $\tau_p = \hbar/k_B T$, constrained by the uncertainty principle between dissipative time scale τ and energy dissipation $E \sim k_B T$, $\tau \cdot k_B T \gtrsim \hbar$. Redefining $\Gamma(T, B)$ as the dissipation energy scale in magnetic field, we can obtain the universal bound of dissipation, $\hbar/\tau_p \sim \Gamma(T, B)$. Our experimental observation in $\Gamma(T, B)$ scaling for the inelastic scattering gives a linear relation, $\hbar/\tau = A\Gamma(T, B)$ with $A = 1.80$, in good agreement with expected behavior.

Upon increasing temperatures, we observe a crossover of the scattering mechanism in the resistivity from T -

linear Planckian dissipation to another underlying scattering rate, suggesting that the Planckian bound indeed limits the charge transport at low temperatures (the lower inset of fig. 1a). The underlying scattering rate is well-described by a linear term due to phonons and a $T^{5/3}$ -term expected in three-dimensional FM QC systems [2]. The $T^{5/3}$ -resistivity is similarly observed in BaCo_2As_2 (see SM), hinting at the correlation between QC behavior and the $3d^7$ configuration.

Notwithstanding the quasi-two-dimensional layered structure, the NFL magnetotransport is independent of applied field orientations with respect to the FeAs layers. We plot the anisotropy of the MR, $\Delta\rho(B \parallel c)/\Delta\rho(B \parallel ab)$, as a function of temperature in fig. 1d. The anisotropy between transverse MR in the out-of-plane field ($B \parallel c$, $I \parallel ab$) and transverse MR in the in-plane field ($B \parallel ab$, $B \perp I \parallel ab$) decreases down to unity with decreasing temperatures, suggesting the spatial dimension of the system is three. The isotropy in MR remains even at 35 T, as shown in the angular dependence of MR (fig.2 inset). Due to the three dimensionality, we observe similar $\Gamma(T, B)$ scaling in the resistivity regardless of applied field orientations (see SM). Moreover, the observed positive MR appears not to be driven by the orbital effect due to the Lorentz force, but rather associated with Zeeman energy-tuned scattering, evidenced by the isotropy in the MR between in-plane transverse ($B \parallel c$, $I \parallel ab$) and longitudinal ($B \parallel I \parallel ab$) configurations (fig.1d).

In addition to resistivity, magnetic susceptibility $\chi = M/B$ and electronic heat capacity C_e/T also exhibit canonical NFL behavior, i.e., diverging temperature dependence associated with QC instabilities [5]. The magnetic susceptibility varies as $\chi \propto T^{-1/3}$ at low temperatures below 8 K (inset of fig. 2a), in contrast to the T -independent Pauli paramagnetic susceptibility $\chi_p = 2g\mu_B^2 D(E_F)$ (with electron g -factor and density of states at the Fermi energy $D(E_F)$) observed in FL metals, and observed upon increasing magnetic field to 7 T (fig.2a). A similar crossover is also observed in the heat capacity. Obtained from the subtraction of phonon (C_{ph}) and nuclear Schottky contributions (C_{Sch}) from the total heat capacity (C_{tot}), the electronic specific heat coefficient $C_e/T = (C_{tot} - C_{ph} - C_{Sch})/T$ exhibits power law divergence stronger than logarithmic in the temperature dependence down to ~ 150 mK (fig.2b). Diminished with applying field, the NFL behavior observed in zero field completely disappears at applied field of 10 T, indicative of the recovery of FL. We note that the obtained specific heat coefficient $\gamma = C_e/T$ at $B = 0$ T, combined with the magnetic susceptibility χ , provides large Wilson ratio $R_W = \pi^2 k_B^2 \chi / 3\mu_B^2 \gamma = 3.2$ at $T = 1.8$ K, suggestive of the presence of magnetic instabilities similar to BaCo_2As_2 .

The observation of FL recovery with magnetic field corroborates the presence of a new energy scale $k_B T^*$,

distinctive of crossover between the QC ($k_B T \gg g\mu_B B$) and FL ($k_B T \ll g\mu_B B$) regimes. Intriguingly, this new energy scale allows a single scaling function of T/B in the magnetization, written by,

$$-\frac{dM}{dT} = B^{-\frac{1}{3}} f_M \left(\frac{T}{B} \right), \quad (1)$$

as shown in fig.2c. This scaling relation indeed reveals the underlying free energy given by a universal function of T/B ,

$$F(T, B) = B^{(d+z)/y_b} f_F \left(\frac{T}{B^{z/y_b}} \right), \quad (2)$$

where d is the spatial dimensionality, z is the dynamic exponent, and y_b is the scaling exponent related to the tuning parameter B , alternatively written in terms of the correlation length exponent ν , namely, $z/y_b = z\nu$ [1–3, 34]. Here, $f_F(x)$ is a universal function of x . Hence, the magnetization can be derived from the derivative of the free energy,

$$-\frac{dM}{dT} = -\frac{d}{dT} \left(\frac{dF}{dB} \right) = B^{d/y_b-1} f_M \left(\frac{T}{B^{z/y_b}} \right). \quad (3)$$

Directly comparing this with the observed QC scaling relation in fig. 2c, we can extract the critical exponents in the free energy, namely, $z/y_b = 1$ and $d/y_b - 1 = -1/3$, yielding $z\nu = 1$ and $d/z = 2/3$. These values of the critical exponents describe the specific heat by using the same free energy,

$$\frac{C_e(B, T)}{T} = -\frac{\partial^2 F}{\partial T^2} = B^{\frac{d-z}{y_b}} f_C \left(\frac{T}{B^{z/y_b}} \right). \quad (4)$$

Rewriting the free energy, $F(T, B) = B^{\frac{d+z}{y_b}} f(T/B^{z/y_b}) = T^{\frac{d+z}{z}} \tilde{f}(B/T^{y_b/z})$, we find

$$\frac{\Delta C_e(T, B)}{T} = \frac{C_e(T, B)}{T} - \frac{C_e(T, 0)}{T} = B^{-\frac{1}{3}} g_C \left(\frac{T}{B} \right), \quad (5)$$

where $g_C(x)$ is field-dependent part of $f_C(x)$ (see SM). As demonstrated in fig. 2d, this expression illustrates scale invariance in the specific heat that persists over nearly three order of magnitude in the scaling variable T/B .

The T/B scaling in thermodynamics clearly discloses the presence of the QCP located exactly at zero field and absolute zero, similar to the layered QC metals YbAlB₄ [35] and YFe₂Al₁₀ [36]. More notably, the multi-band nature in iron pnictides affixes the uniqueness of quantum criticality for Ba(Fe_{1/3}Co_{1/3}Ni_{1/3})₂As₂. Dominated by electron-like carriers, the Hall resistivity ρ_{yx} is negative and perfectly linear in field at high temperatures ($T = 20$ K) as shown in fig.3a. Upon cooling, ρ_{yx} develops a non-linearity with negative curvature. More prominent below 1 K, the non-linear Hall resistivity switches its sign at

low fields below 2 T. The sign change is more readily observed in the temperature dependence of Hall coefficient R_H defined by ρ_{yx}/B at low- T and low- H region (fig.3b), implying the emergence of hole-like carriers in the vicinity of the QCP. The radial shape of this emergence in the field-temperature phase diagram confirms the absence of an intrinsic energy scale in R_H (fig. 3c), or in other words, the presence of scale invariance in the Hall effect tuned by temperature and magnetic field. Similar to the resistivity, R_H obeys $\Gamma(T, B)$ scaling (fig. 3d), consolidating the existence of scale invariance near the quantum critical point in this system beyond any doubt.

Angle-resolved photoemission measurements identify a unique electronic structure and confirm the anomalous scattering rate correlated with Planckian dissipation. Unlike heavily electron-doped BaCo₂As₂, the electronic structure for Ba(Fe_{1/3}Co_{1/3}Ni_{1/3})₂As₂ consists of a large hole-like pocket and a cross-shaped electron-like Fermi surface around the Γ point together with oval and elongated electron pockets around the M points, exhibited by the Fermi surface map (fig.4a), the band dispersion along $k_x = 0$ direction (fig. 4b) at 30K, and a schematic illustration (fig. 4a, inset). The elongated electron pockets are very shallow, and the chemical potential is located close to the bottom of the shallow bands. Dominating transport at low temperatures and fields, the large hole-like pocket is identified as the one responsible for quantum critical behavior. Amazingly, the scattering rate (obtained from the dispersion of the hole-like bands at 1 K) varies linearly with the kinetic energy up to 100 meV, consistent with Planckian dissipation as observed in the resistivity (fig. 4c and d).

While our primary observations of the scale invariance in the thermodynamics are consistent with quantum criticality overall, they indicate a highly unusual critical behavior in Ba(Fe_{1/3}Co_{1/3}Ni_{1/3})₂As₂. While sharing an enhancement of the Wilson ratio with BaCo₂As₂ and $T^{5/3}$ transport scattering rate indicative of a FM instability, the critical behavior in Ba(Fe_{1/3}Co_{1/3}Ni_{1/3})₂As₂ is not described by any known theoretical predictions. Assuming spacial dimensionality of three based on the observed isotropic response in MR and magnetization (see SM), the observed critical exponents of $d/z = 2/3$ and $z\nu = z/y_b = 1$ yield $z = 4.5$ and $\nu = 2/9$, which do not match the predictions for either mean-field Hertz-Moriya-Millis theory for $d = 3$ (which predict $z = 3$ for clean FM and $z = 4$ for dirty FM quantum criticality with $\nu = 1/2$) [1–3], or predictions beyond mean-field, which predict the appearance of a weak first-order transition instead of new critical exponents [37–39]. Experimentally, previously measured exponents in QC materials, such as YbNi₄(P_{1-x}As_x)₂ (FM QCP, $\nu z \sim 5$) [40], CeCu_{6-x}Au_x (AFM QCP, $d/z = 1/4$, $\nu z = 1$) [41], β -YbAlB₄ (mixed-valence metal, $d/z = 1/2$, $\nu z = 1$) [35], YFe₂Al₁₀ (layered QC metal, $d/z = 1$, $\nu z = 0.59$ [36]), and Sr_{0.3}Ca_{0.7}RuO₃ (disordered FM QCP, $z = 1.76$) [42], are also incom-

patible with our observations, indicating highly unusual dynamical critical behavior in this material.

Indeed, the anomalous behavior observed in $\text{Ba}(\text{Fe}_{1/3}\text{Co}_{1/3}\text{Ni}_{1/3})_2\text{As}_2$ is more prominent than that observed in both of the end members of the $3d^7$ configuration line, namely, BaCo_2As_2 and $\text{Ba}(\text{Fe,Ni})_2\text{As}_2$ (see SM), signifying that the specific 1/3 equal ratios of Fe:Co:Ni in BaCo_2As_2 are indeed important to stabilizing a unique quantum critical ground state. In fact, as shown in fig. 5, the observed NFL scattering behavior in $\text{Ba}(\text{Fe}_{1/3}\text{Co}_{1/3}\text{Ni}_{1/3})_2\text{As}_2$ is completely robust against pressure and even replacement of Ba for Sr (i.e. in $\text{Sr}(\text{Fe}_{1/3}\text{Co}_{1/3}\text{Ni}_{1/3})_2\text{As}_2$), implying either an electronic structure modification beyond d -electron tuning, or a significant role for transition metal site dilution. The peculiarity of critical behavior can also be highlighted by the high residual scattering rate due to random disorder (see SM). While generally obscuring the critical behavior, high disordered states play an important role in some quantum critical materials, such as high entropy alloys [43, 44], in which similar NFL behavior has been realized [43, 44]. Indeed, the pressure insensitivity of the T -linear scattering in $\text{Ba}(\text{Fe}_{1/3}\text{Co}_{1/3}\text{Ni}_{1/3})_2\text{As}_2$ implies disorder is a key ingredient to tune the quantum criticality. The disorder in this system enhances the residual resistivity ρ_0 in the order of $100 \mu\Omega\text{cm}$, yielding a mean free path $\ell = \hbar(3\pi^2)^{1/3}/n^{2/3}e^2\rho_0 \sim 17 \text{ \AA}$ approaching the lattice constant value $a = 3.99 \text{ \AA}$ (see SM). Together, our experimental observations of Planckian dissipation-limited scattering and scale invariance in this system indicate the realization of a truly novel quantum fluid possibly void of quasiparticles as described by holographic correspondence [11–13], and may provide the key to understanding the lack of superconductivity driven by quantum critical fluctuations.

Experimental research was supported by the National Science Foundation Division of Materials Research Award No. DMR-1610349, and materials development supported by the Gordon and Betty Moore Foundation's EPiQS Initiative through grant no. GBMF4419. A portion of this work was performed at the National High Magnetic Field Laboratory, which is supported by National Science Foundation Cooperative Agreement No. DMR-1157490 and the State of Florida.

[1] Hertz, J. A. Quantum critical phenomena. *Phys. Rev. B* **14**, 1165 (1976).
 [2] Moriya, T. *Spin Fluctuations in Itinerant Electron Magnetism* (Springer-Verlag, 1985).
 [3] Millis, A. J. Effect of a nonzero temperature on quantum critical points in itinerant fermion systems. *Phys. Rev. B* **48**, 7183–7196 (1993).
 [4] Coleman, P. & Schofield, A. J. Quantum criticality. *Nature* **433**, 226–229 (2005).

[5] Stewart, G. Non-fermi-liquid behavior in d - and f -electron metals. *Rev. Mod. Phys.* **73**, 797 (2001).
 [6] Taillefer, L. Scattering and pairing in cuprate superconductors. *Annual Review of Condensed Matter Physics* **1**, 51–70 (2010).
 [7] Shibauchi, T., Carrington, A. & Matsuda, Y. A quantum critical point lying beneath the superconducting dome in iron pnictides. *Annual Review of Condensed Matter Physics* **5**, 113–135 (2014).
 [8] Zaanen, J. Why the temperature is high. *Nature* **430**, 512 EP – (2004).
 [9] Giraldo-Gallo, P. *et al.* Scale-invariant magnetoresistance in a cuprate superconductor. *Science* **361**, 479–481 (2018).
 [10] Legros, A. *et al.* Universal T -linear resistivity and planckian dissipation in overdoped cuprates. *Nature Physics* **15**, 142–147 (2019).
 [11] Hartnoll, S. A., Kovtun, P. K., Müller, M. & Sachdev, S. Theory of the nernst effect near quantum phase transitions in condensed matter and in dyonic black holes. *Phys. Rev. B* **76**, 144502 (2007).
 [12] Hartnoll, S. A. Theory of universal incoherent metallic transport. *Nature Physics* **11**, 54 EP – (2014).
 [13] Patel, A. A., McGreevy, J., Arovas, D. P. & Sachdev, S. Magnetotransport in a model of a disordered strange metal. *Phys. Rev. X* **8**, 021049 (2018).
 [14] Paglione, J. & Greene, R. L. High-temperature superconductivity in iron-based materials. *Nat Phys* **6**, 645 (2010).
 [15] Mazin, I. I., Singh, D. J., Johannes, M. D. & Du, M. H. Unconventional Superconductivity with a Sign Reversal in the Order Parameter of $\text{LaFeAsO}_{1-x}\text{F}_x$. *Phys. Rev. Lett.* **101**, 057003 (2008).
 [16] Kuroki, K., Usui, H., Onari, S., Arita, R. & Aoki, H. Pnictogen height as a possible switch between high- T_c nodeless and low- T_c nodal pairings in the iron-based superconductors. *Phys. Rev. B* **79**, 224511 (2009).
 [17] Chu, J.-H. *et al.* In-Plane Resistivity Anisotropy in an Underdoped Iron Arsenide Superconductor. *Science* **329**, 824–826 (2010).
 [18] Yi, M. *et al.* Symmetry-breaking orbital anisotropy observed for detwinned $\text{Ba}(\text{Fe}_{1-x}\text{Co}_x)_2\text{As}_2$ above the spin density wave transition. *Proceedings of the National Academy of Sciences* **108**, 6878–6883 (2011).
 [19] Nakajima, M. *et al.* Unprecedented anisotropic metallic state in undoped iron arsenide BaFe_2As_2 revealed by optical spectroscopy. *Proceedings of the National Academy of Sciences* **108**, 12238–12242 (2011).
 [20] Chu, J.-H., Kuo, H.-H., Analytis, J. G. & Fisher, I. R. Divergent nematic susceptibility in an iron arsenide superconductor. *Science* **337**, 710–712 (2012).
 [21] Yanagi, H. *et al.* Itinerant ferromagnetism in the layered crystals LaCoOX ($x = \text{P, As}$). *Phys. Rev. B* **77**, 224431 (2008).
 [22] Anand, V. K. *et al.* Crystallography and physical properties of BaCo_2As_2 , $\text{Ba}_{0.94}\text{K}_{0.06}\text{Co}_2\text{As}_2$, and $\text{Ba}_{0.78}\text{K}_{0.22}\text{Co}_2\text{As}_2$. *Phys. Rev. B* **90**, 064517 (2014).
 [23] Wiecki, P. *et al.* Competing Magnetic Fluctuations in Iron Pnictide Superconductors: Role of Ferromagnetic Spin Correlations Revealed by NMR. *Phys. Rev. Lett.* **115**, 137001 (2015).
 [24] Wiecki, P., Ogloblichev, V., Pandey, A., Johnston, D. C. & Furukawa, Y. Coexistence of antiferromagnetic and ferromagnetic spin correlations in SrCo_2As_2 revealed by ^{59}Co and ^{75}As NMR. *Phys. Rev. B* **91**, 220406 (2015).
 [25] Sefat, A. S. *et al.* Renormalized behavior and proximity

- of BaCo₂As₂ to a magnetic quantum critical point. *Phys. Rev. B* **79**, 024512 (2009).
- [26] Sefat, A. S. *et al.* Structure and anisotropic properties of BaFe_{2-x}Ni_xAs₂ ($x = 0, 1,$ and 2) single crystals. *Phys. Rev. B* **79**, 094508 (2009).
- [27] Eckberg, C. *et al.* Evolution of structure and superconductivity in Ba(Ni_{1-x}Co_x)₂As₂. *Phys. Rev. B* **97**, 224505 (2018).
- [28] Ni, N. *et al.* Phase diagrams of Ba(Fe_{1-x}M_x)₂As₂ single crystals ($M = \text{Rh}$ and Pd). *Phys. Rev. B* **80**, 024511 (2009).
- [29] Canfield, P. C., Bud'ko, S. L., Ni, N., Yan, J. Q. & Kracher, A. Decoupling of the superconducting and magnetic/structural phase transitions in electron-doped BaFe₂As₂. *Phys. Rev. B* **80**, 060501 (2009).
- [30] Liu, C. *et al.* Evidence for a Lifshitz transition in electron-doped iron arsenic superconductors at the onset of superconductivity. *Nat Phys* **6**, 419–423 (2010).
- [31] Neupane, M. *et al.* Electron-hole asymmetry in the superconductivity of doped BaFe₂As₂ seen via the rigid chemical-potential shift in photoemission. *Phys. Rev. B* **83**, 094522 (2011).
- [32] Hayes, I. M. *et al.* Scaling between magnetic field and temperature in the high-temperature superconductor BaFe₂(As_{1-x}P_x)₂. *Nat Phys* **12**, 916–919 (2016).
- [33] Sutherland, M. *et al.* Transport and thermodynamic evidence for a marginal Fermi-liquid state in ZrZn₂. *Phys. Rev. B* **85**, 035118 (2012).
- [34] Sachdev, S. *Quantum Phase Transitions* (Cambridge University Press, Cambridge, UK, 1999).
- [35] Matsumoto, Y. *et al.* Quantum Criticality Without Tuning in the Mixed Valence Compound $\beta\text{-YbAlB}_4$. *Science* **331**, 316–319 (2011).
- [36] Wu, L. S., Kim, M. S., Park, K., Tsvetlik, A. M. & Aronson, M. C. Quantum critical fluctuations in layered YFe₂Al₁₀. *Proceedings of the National Academy of Sciences* **111**, 14088–14093 (2014).
- [37] Belitz, D., Kirkpatrick, T. R. & Vojta, T. Nonanalytic behavior of the spin susceptibility in clean fermi systems. *Phys. Rev. B* **55**, 9452–9462 (1997).
- [38] Rech, J., Pépin, C. & Chubukov, A. V. Quantum critical behavior in itinerant electron systems: Eliashberg theory and instability of a ferromagnetic quantum critical point. *Phys. Rev. B* **74**, 195126 (2006).
- [39] Conduit, G. J., Green, A. G. & Simons, B. D. Inhomogeneous phase formation on the border of itinerant ferromagnetism. *Phys. Rev. Lett.* **103**, 207201 (2009).
- [40] Steppke, A. *et al.* Ferromagnetic quantum critical point in the heavy-fermion metal YbNi₄(P_{1-x}As_x)₂. *Science* **339**, 933–936 (2013).
- [41] Schroeder, A. *et al.* Onset of antiferromagnetism in heavy-fermion metals. *Nature* **407**, 351 (2000).
- [42] Huang, C. L. *et al.* Anomalous quantum criticality in an itinerant ferromagnet. *Nat Commun* **6** (2015).
- [43] Sales, B. C. *et al.* Quantum critical behavior in a concentrated ternary solid solution. *Scientific Reports* **6**, 26179 EP – (2016).
- [44] Sales, B. C. *et al.* Quantum critical behavior in the asymptotic limit of high disorder in the medium entropy alloy NiCoCr_{0.8}. *npj Quantum Materials* **2**, 33 (2017).
- [45] Momma, K. & Izumi, F. VESTA3 for three-dimensional visualization of crystal, volumetric and morphology data. *Journal of Applied Crystallography* **44**, 1272–1276 (2011).

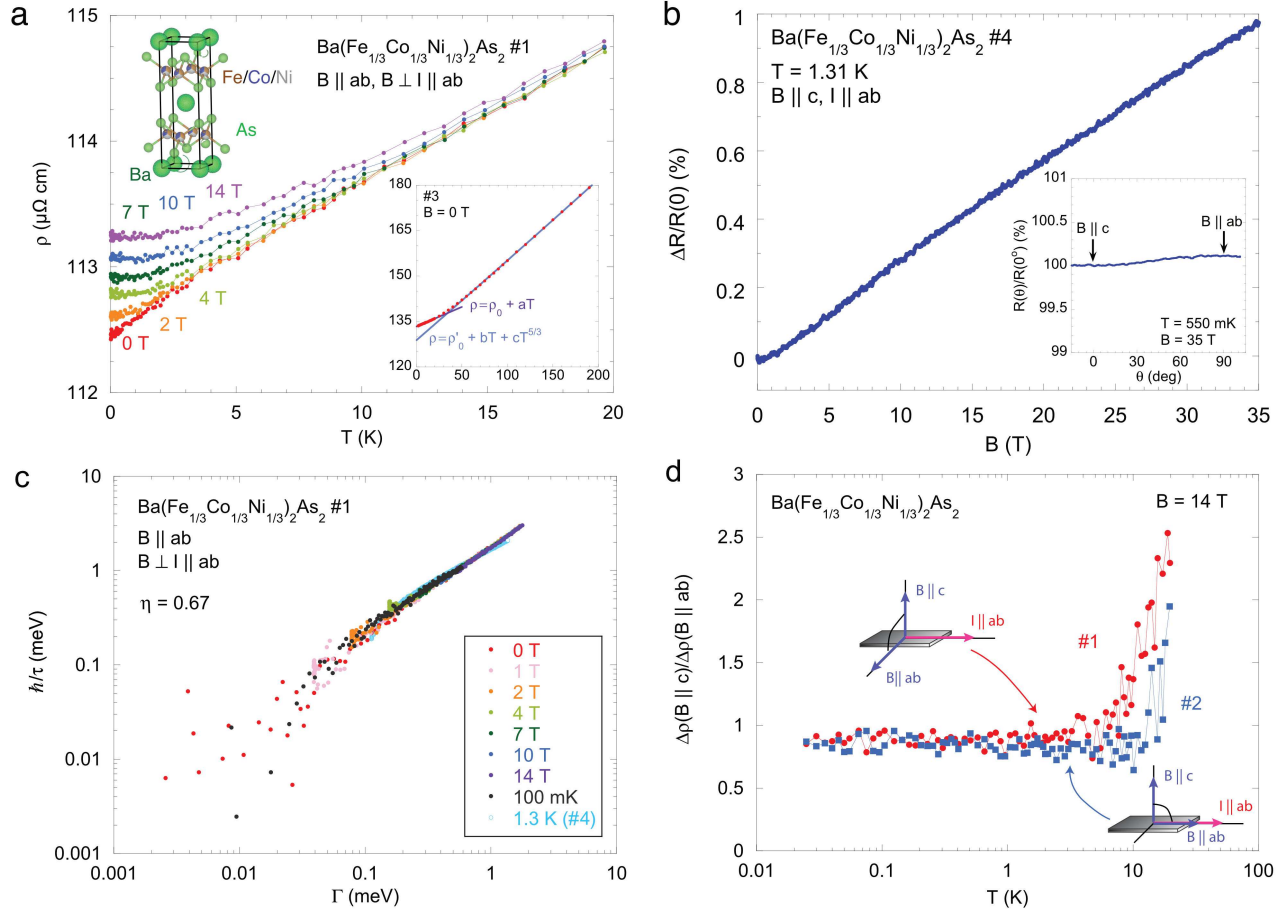


FIG. 1: **Planckian dissipation and scale invariance in the resistivity of $\text{Ba}(\text{Fe}_{1/3}\text{Co}_{1/3}\text{Ni}_{1/3})_2\text{As}_2$.** **a**, Temperature dependence of resistivity for $\text{Ba}(\text{Fe}_{1/3}\text{Co}_{1/3}\text{Ni}_{1/3})_2\text{As}_2$ in the configuration of $B \parallel ab, B \perp I \parallel ab$. Upper inset: Crystal structure for $\text{Ba}(\text{Fe}_{1/3}\text{Co}_{1/3}\text{Ni}_{1/3})_2\text{As}_2$ [45]. Lower inset: Crossover from underlying phonon ($\propto T$) and FM ($\propto T^{5/3}$) scattering to Planckian dissipation limit ($\propto k_B T$). Solid lines are fits to the data using $\rho = \rho_0 + aT$ at low temperatures below ~ 30 K and $\rho = \rho'_0 + bT + cT^{5/3}$ at high temperatures above ~ 50 K. **b**, Magnetic field dependence of $\Delta R(B)/R(0) \equiv (R(1.31 \text{ K}, B) - R(1.31 \text{ K}, 0))/R(1.31 \text{ K}, 0)$ at $T = 1.31$ K. Inset: Angular dependence of magnetoresistance at $T = 550$ mK and $B(\parallel c \perp I) = 35$ T. **c**, Inelastic scattering rate \hbar/τ as a function of $\Gamma = \sqrt{(k_B T)^2 + (\eta \mu_B B)^2}$ with $\eta = 0.67$, suggestive of Planckian dissipation dominating the scattering mechanism in $\text{Ba}(\text{Fe}_{1/3}\text{Co}_{1/3}\text{Ni}_{1/3})_2\text{As}_2$. **d**, Temperature dependence of anisotropy of magnetoresistance between $\Delta\rho(B \parallel c)$ and $\Delta\rho(B \parallel ab \perp I)$ (sample #1) and between $\Delta\rho(B \parallel c)$ and $\Delta\rho(B \parallel ab \parallel I)$ (sample #2) at $B = 14$ T, showing lack of anisotropy in the scattering rate.

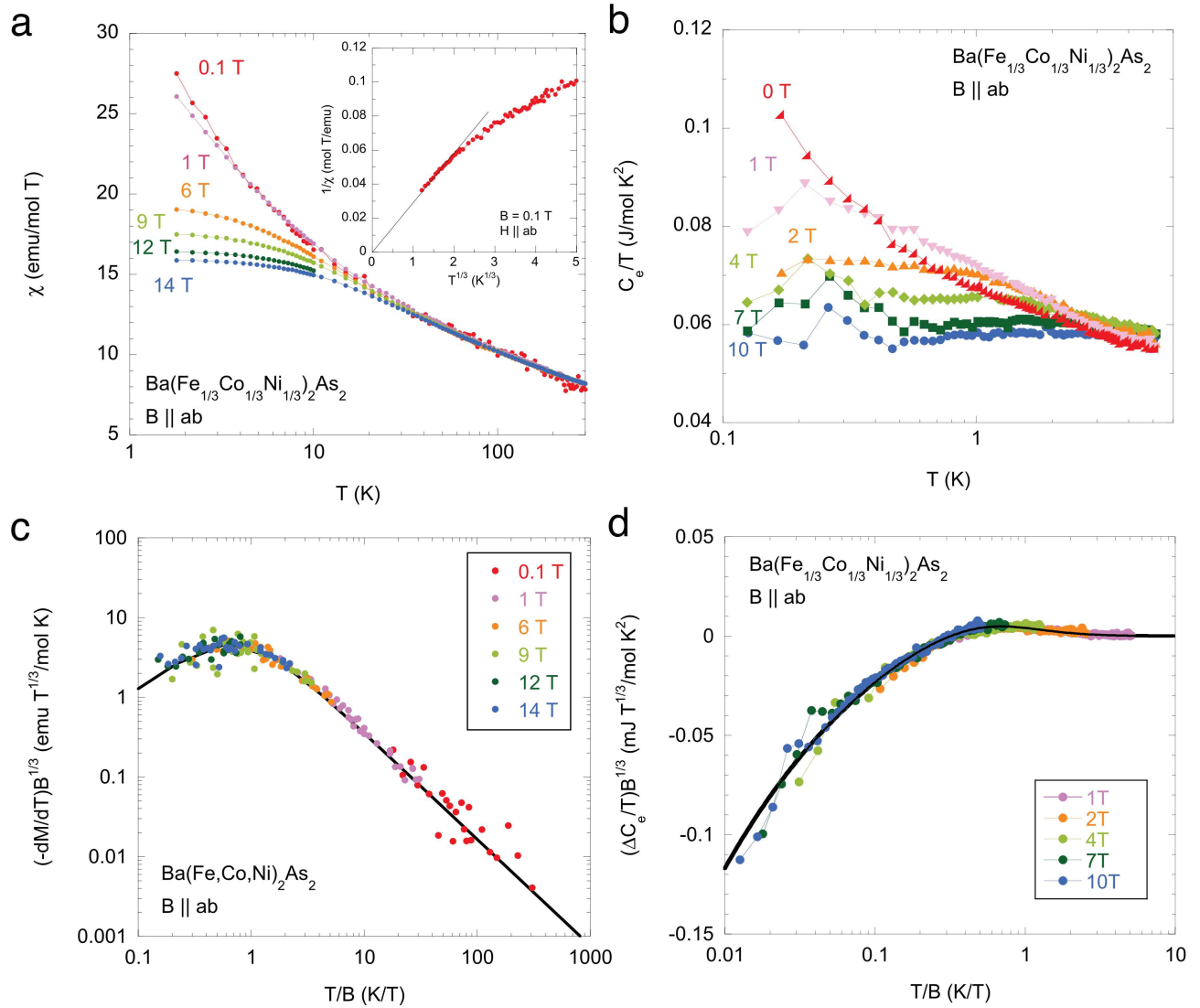


FIG. 2: Non-Fermi liquid to Fermi liquid crossover and scale invariance in thermodynamic quantities. **a**, Temperature dependence of magnetic susceptibility for $\text{Ba}(\text{Fe}_{1/3}\text{Co}_{1/3}\text{Ni}_{1/3})_2\text{As}_2$ ($B \parallel ab$). Inset: $1/\chi$ as a function of $T^{1/3}$ at low temperatures. **b**, Electronic specific heat $C_e/T = (C_{tot} - C_{sch} - C_{lat})/T$ for $\text{Ba}(\text{Fe}_{1/3}\text{Co}_{1/3}\text{Ni}_{1/3})_2\text{As}_2$ under several fields parallel to ab -plane. **c**, Temperature-magnetic field scale invariance in magnetization and **d**, specific heat. The measured magnetization and specific heat collapse onto universal scaling curves in the forms of $-dM/dT = B^{-1/3}f_M(T/B)$ and $\Delta C_e/T = B^{-1/3}g_C(T/B)$, respectively, indicating the presence of the underlying free energy given by a universal function of T/B and the existence of the QCP located at $T = 0$ and $B = 0$. Black lines represent scaling functions $f_M(T/B)$ for magnetization and $g_C(T/B)$ for specific heat derived from the underlying free energy, described in the main text.

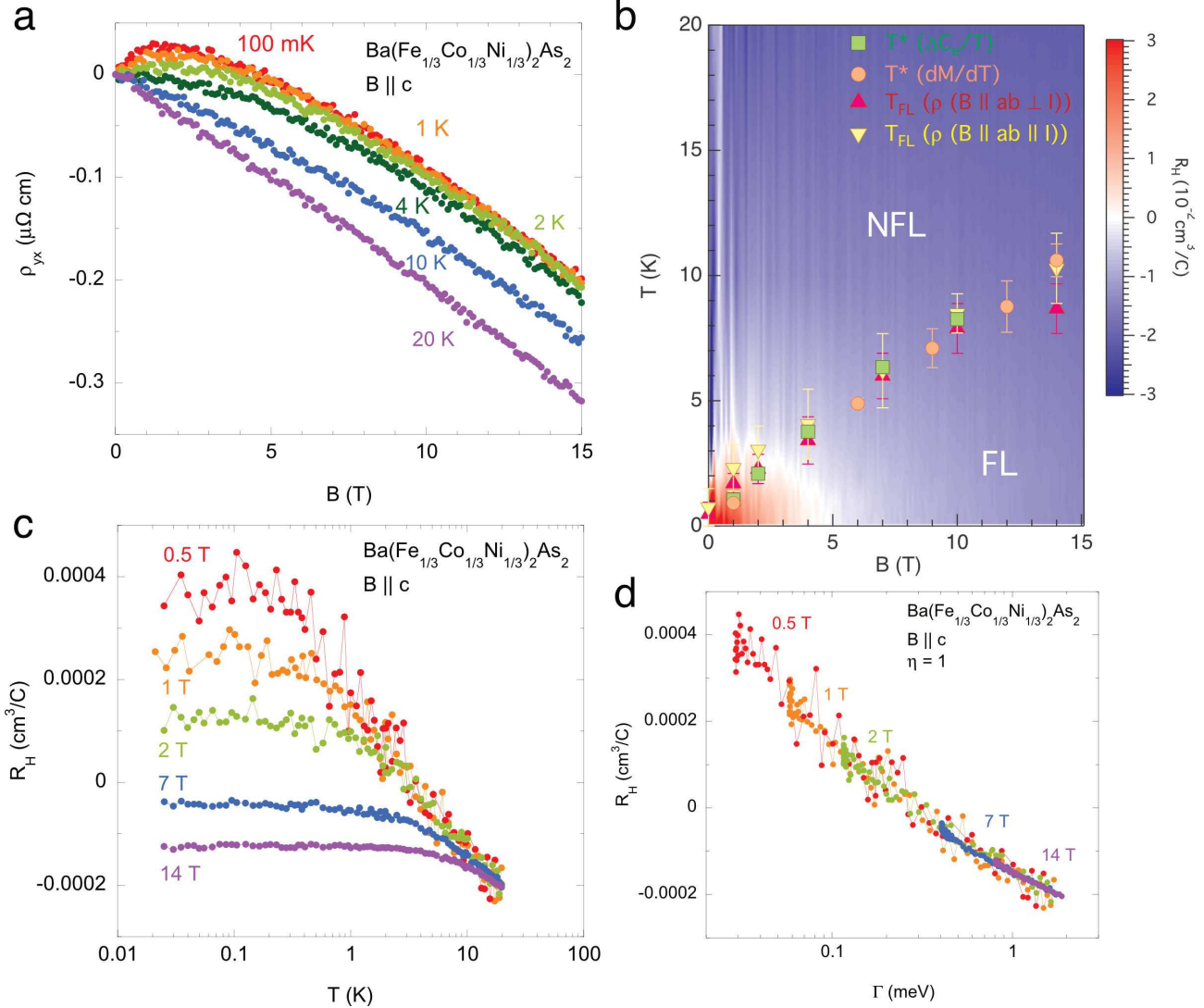


FIG. 3: **Emergence of hole-like carriers near the quantum critical point and scale invariance in Hall effect.** **a**, Hall resistivity ρ_{yx} as a function of B . At high temperatures, ρ_{yx} is negative and linear in field. Upon cooling temperatures, ρ_{yx} becomes non-linear and its sign switches to positive at low fields below 2 T. **b**, Temperature dependence of Hall coefficient R_H defined by ρ_{yx}/B . **c**, $T - B$ phase diagram with color plot of R_H . Crossover temperatures T^* obtained from the quantum scaling in dM/dT and $\Delta C_e/T$ and T_{FL} from the T^2 -fit are also plotted in the phase diagram. **d**, R_H as a function of $\Gamma(T, B) \equiv \sqrt{(k_B T)^2 + (\eta \mu_B B)^2}$ with $\eta = 1$. All the data collapse onto one universal curve, suggesting unusual scaling between temperature and applied field similar to that found in the longitudinal resistivity.

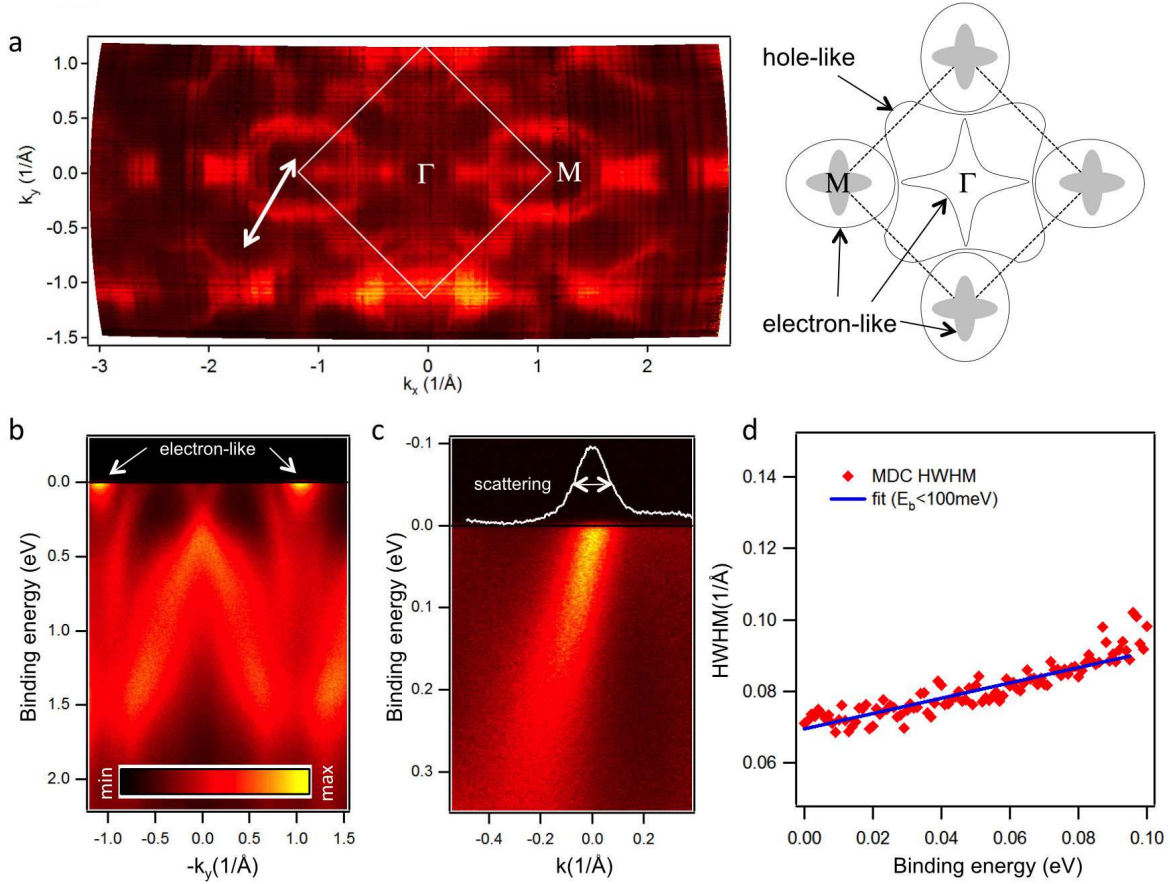


FIG. 4: **Fermi surfaces and anomalous scattering rates in $\text{Ba}(\text{Fe}_{1/3}\text{Co}_{1/3}\text{Ni}_{1/3})_2\text{As}_2$.** **a**, Angle-resolved photoemission study of Fermi surface map for $\text{Ba}(\text{Fe}_{1/3}\text{Co}_{1/3}\text{Ni}_{1/3})_2\text{As}_2$, measured at 30 K. White lines denote the Brillouin zone (BZ) boundary, and white arrow corresponds to the cut shown in panel **c**. The inset depicts a schematic Fermi surface corresponding to the experimentally observed data, with shallow elongated electron pockets shown in gray. **b**, Energy cut along the $k_x = 0$ direction, highlighting the elongated shallow electron-like pockets observed near the BZ corners. **c**, Energy dispersion of hole-like pocket measured at 1 K near the BZ boundary along the cut indicated by white arrow in panel **a**, where sharp crossings of the Fermi level are found. The momentum axis originates at the crossing point. The white spectrum is the momentum distribution curve at the Fermi level, with indicated width a representative measure of the scattering rate. **d**, Scattering rate energy dependence obtained from the width of energy dispersion in panel **c**, with linear fit up to 100 meV.

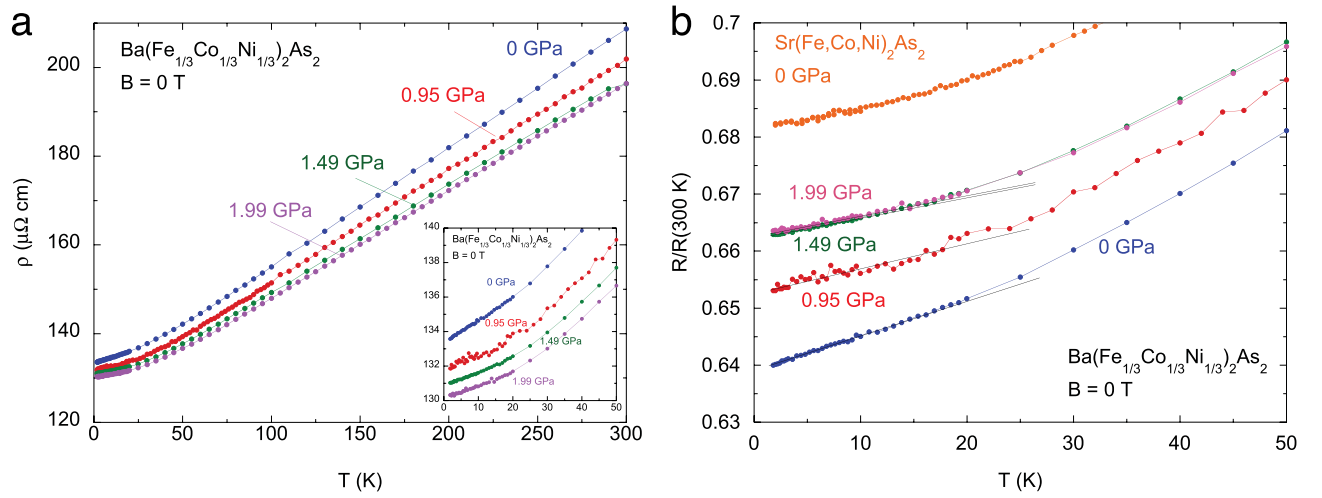


FIG. 5: **Robust non-Fermi liquid behavior against pressure.** **a**, Overall temperature dependence of resistivity for Ba(Fe_{1/3}Co_{1/3}Ni_{1/3})₂As₂ under applied pressure. The linear- T resistivity below 20 K is robust against applying pressure up to 1.99 GPa as shown in the inset. **b**, Normalized resistance $R/R(300$ K) vs T under pressure. On applying pressure, $R/R(300$ K) for Ba(Fe_{1/3}Co_{1/3}Ni_{1/3})₂As₂ increases, approaching that for Sr(Fe_{1/3}Co_{1/3}Ni_{1/3})₂As₂ with smaller lattice constants than Ba(Fe_{1/3}Co_{1/3}Ni_{1/3})₂As₂ (see SM), indicative of robustness of linear- T behavior in the resistivity against pressure.

Supplementary Materials: Planckian dissipation and scale invariance in a quantum-critical disordered pnictide

GROWTH AND CHARACTERIZATION

The samples of $\text{Ba}(\text{Fe}_{1/3}\text{Co}_{1/3}\text{Ni}_{1/3})_2\text{As}_2$ were grown by *TMA*s ($TM = \text{Fe}, \text{Co}, \text{and Ni}$) self-flux method with the molar ratios of 3:4:4:4 = Ba:FeAs:CoAs:NiAs. Resulting crystals were cleaved out of the flux. The typical crystal size is $5 \times 5 \times 0.1 \text{ mm}^3$.

The lattice constants a and c for $\text{Ba}(\text{Fe}_{1/3}\text{Co}_{1/3}\text{Ni}_{1/3})_2\text{As}_2$ were determined by x-ray diffraction with $\text{Cu-}K_\alpha$ radiation, plotted together with $ATM_2\text{As}_2$ ($A = \text{Sr and Ba}, TM = \text{Fe, Co and Ni}$) as a function of d configurations (fig.S1). Sharing the same d configuration with each other, the lattice parameter c for $\text{Ba}(\text{Fe}_{1/3}\text{Co}_{1/3}\text{Ni}_{1/3})_2\text{As}_2$ is similar to those for BaCo_2As_2 and $\text{Ba}(\text{Fe,Ni})_2\text{As}_2$, while a has a large variation by 1% among them.

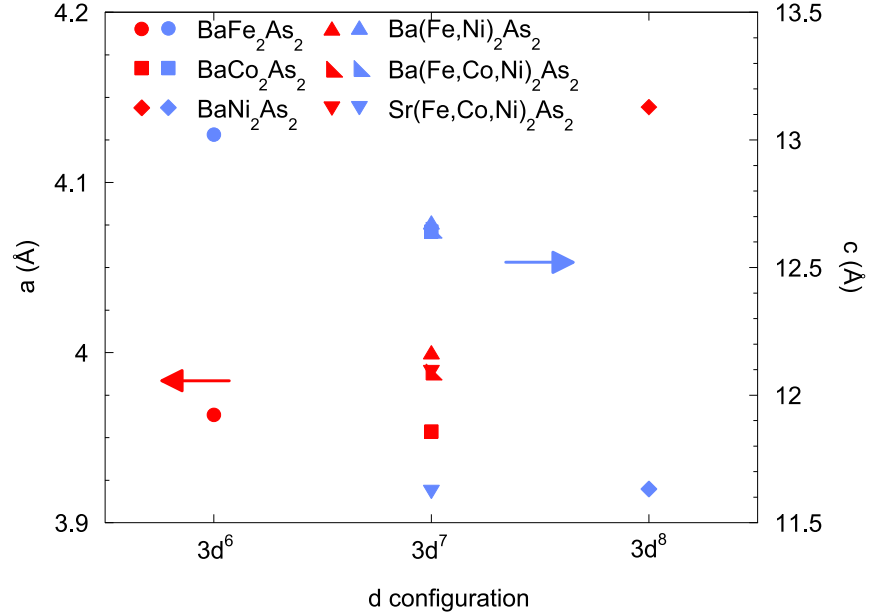


FIG. S1: **Lattice constant of $ATM_2\text{As}_2$ ($A = \text{Ba}, \text{Sr}, TM = \text{Fe,Co,Ni}$).** Lattice parameters a (red) and c (blue) as a function of $3d$ configurations for BaFe_2As_2 , BaCo_2As_2 , $\text{Ba}(\text{Fe}_{1/3}\text{Co}_{1/3}\text{Ni}_{1/3})_2\text{As}_2$, $\text{Ba}(\text{Fe,Ni})_2\text{As}_2$, BaNi_2As_2 , represented by filled circles, and $\text{Sr}(\text{Fe}_{1/3}\text{Co}_{1/3}\text{Ni}_{1/3})_2\text{As}_2$, represented by squares.

SINGLE CRYSTAL REFINEMENTS

Single-crystal x-ray diffraction was performed at 150 K and 250 K for $\text{Ba}(\text{Fe}_{1/3}\text{Co}_{1/3}\text{Ni}_{1/3})_2\text{As}_2$ and at 250 K for $\text{Sr}(\text{Fe}_{1/3}\text{Co}_{1/3}\text{Ni}_{1/3})_2\text{As}_2$ with Bruker APEX-II CCD system equipped with a graphite monochromator and a MoKa sealed tube ($\lambda = 0.71073 \text{ \AA}$). The crystallographic data obtained from refinements for $\text{Ba}(\text{Fe}_{1/3}\text{Co}_{1/3}\text{Ni}_{1/3})_2\text{As}_2$ and $\text{Sr}(\text{Fe}_{1/3}\text{Co}_{1/3}\text{Ni}_{1/3})_2\text{As}_2$ are summarized in Table 1. Note that the final indices of the refinements R_1 are 1.01 % (Ba at 250 K), 1.12 % (Ba at 150 K), and 1.58 % (Sr at 250 K), close to the best values for Ba 122 crystals [1], indicative of the high quality samples in which the doped transition metals are randomly distributed and do not form the clusters.

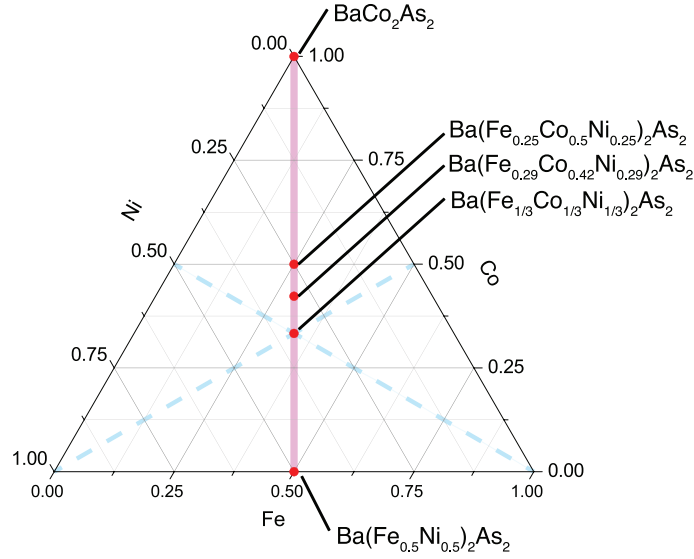


FIG. S2: **Ternary phase diagram.** A ternary phase diagram for $\text{Ba}(\text{Fe},\text{Co},\text{Ni})_2\text{As}_2$. The red circles indicating the locations of BaCo_2As_2 , $\text{Ba}(\text{Fe}_{0.25}\text{Co}_{0.5}\text{Ni}_{0.25})_2\text{As}_2$, $\text{Ba}(\text{Fe}_{0.29}\text{Co}_{0.42}\text{Ni}_{0.29})_2\text{As}_2$, $\text{Ba}(\text{Fe}_{1/3}\text{Co}_{1/3}\text{Ni}_{1/3})_2\text{As}_2$, and $\text{Ba}(\text{Fe}_{0.5}\text{Ni}_{0.5})_2\text{As}_2$, determined by energy dispersion spectroscopy.

TABLE I: Crystallographic data for $A(\text{Fe}_{1/3}\text{Co}_{1/3}\text{Ni}_{1/3})_2\text{As}_2$ ($A = \text{Ba}, \text{Sr}$) determined by single-crystal x-ray diffraction.

	Ba	Ba	Sr
Temperature	250 K	150 K	250 K
Structure	tetragonal	tetragonal	tetragonal
Space group	I4/mmm	I4/mmm	I4/mmm
a (Å)	3.9920(3)	3.9826(3)	3.9885(8)
c (Å)	12.6191(8)	12.6269(10)	11.621(5)
V (Å ³)	201.10(3)	200.28(3)	184.87(9)
Z (formula unit/unit cell)	2	2	2
R_1 ($I \geq 2\sigma(I)$)	0.0101	0.0112	0.0158
wR_2 (all data)	0.0251	0.0264	0.0344
Atomic coordinates (Wyckoff):			
Ba/Sr (2a)	0, 0, 0	0, 0, 0	0, 0, 0
Fe/Co/Ni (4d)	0.5, 0, 0.25	0.5, 0, 0.25	0.5, 0, 0.25
As (4e)	0.5, 0.5, 0.35160(3)	0.5, 0.5, 0.35171(3)	0.5, 0.5, 0.35840(7)
Isotropic displacement parameters U_{eq} (Å ²):			
Ba/Sr	0.01058(8)	0.00740(8)	0.0122(2)
Fe/Co/Ni	0.00961(10)	0.00681(10)	0.0133(2)
As	0.00913(9)	0.00649(9)	0.01224(19)
Bond lengths (Å):			
Ba/Sr-As	3.3875(3)	3.3818(3)	3.2653(7)
Fe/Co/Ni-As	2.3723(2)	2.3695(2)	2.3588(6)
Fe/Co/Ni-Fe/Co/Ni	2.8228(2)	2.8161(2)	2.8203(4)
Bond angles (deg):			
As-Fe/Co/Ni-As	114.575(16)	114.362(15)	115.44(4)
As-Fe/Co/Ni-As	106.981(7)	107.083(7)	106.57(2)

TERNARY PHASE DIAGRAM AND POSSIBLE COMPETING PHASE

Figure S2 shows a ternary phase diagram for $\text{Ba}(\text{Fe},\text{Co},\text{Ni})_2\text{As}_2$ with red circles indicating the locations of BaCo_2As_2 , $\text{Ba}(\text{Fe}_{0.25}\text{Co}_{0.5}\text{Ni}_{0.25})_2\text{As}_2$, $\text{Ba}(\text{Fe}_{0.29}\text{Co}_{0.42}\text{Ni}_{0.29})_2\text{As}_2$, $\text{Ba}(\text{Fe}_{1/3}\text{Co}_{1/3}\text{Ni}_{1/3})_2\text{As}_2$, and $\text{Ba}(\text{Fe}_{0.5}\text{Ni}_{0.5})_2\text{As}_2$. Determined by energy dispersion spectroscopy, the compositions of Fe, Co, and Ni allow the samples to hold $3d^7$ con-

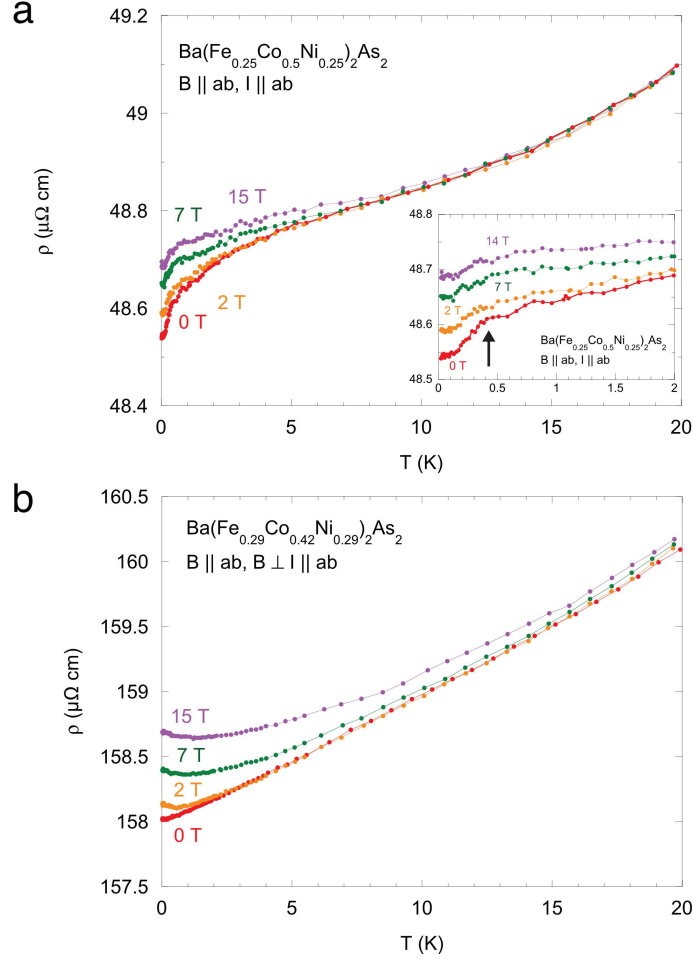


FIG. S3: **Resistivity for Ba(Fe,Co,Ni)₂As₂.** **a**, temperature dependence of resistivity for Ba(Fe_{0.25}Co_{0.5}Ni_{0.25})₂As₂. A resistive kink possibly involving a phase transition is observed at 400 mK. The transition temperature is robust against applying field. **b**, temperature dependence of resistivity for Ba(Fe_{0.29}Co_{0.42}Ni_{0.29})₂As₂, showing non-Fermi liquid behavior at zero field, diminished with magnetic field.

figuration. Interestingly, the very-low-temperature charge transport for Ba(Fe_{0.25}Co_{0.5}Ni_{0.25})₂As₂ reveals a resistive kink at 400 mK, possibly associated with a phase transition (fig. S3a), robust against magnetic fields, while that for Ba(Fe_{0.25}Co_{0.5}Ni_{0.25})₂As₂ shows linear T behavior, suppressed with applying field (fig. S3b).

Heavily electron doped Ba(Fe,Ni)₂As₂, assumedly sharing the same $3d^7$ configuration with BaCo₂As₂ and Ba(Fe_{1/3}Co_{1/3}Ni_{1/3})₂As₂, also shows non-Fermi liquid behavior in the magnetic susceptibility. As shown in fig. S4a, the susceptibility divergetly increases with decreasing temperatures, followed by the saturation below 10 K even at $B = 0$ T. This saturation at finite temperatures implies Ba(Fe,Ni)₂As₂ is located slightly away from a QCP. The non-Fermi liquid temperature dependence is strongly suppressed with applying magnetic field, indicative of the recovery of Fermi liquid regime at the applied field of 14 T. Similar to Ba(Fe_{1/3}Co_{1/3}Ni_{1/3})₂As₂, the crossover from Fermi liquid to non-Fermi liquid indeed allows the quantum critical scaling in the magnetization with the critical exponents of $d/z = 2/3$ and $z\nu = 0.8$, while the obtained $z\nu$ is slightly different from that for Ba(Fe_{1/3}Co_{1/3}Ni_{1/3})₂As₂.

NON-FERMI LIQUID TO FERMI LIQUID CROSSOVER IN THE RESISTIVITY

The Non-Fermi liquid behavior in the temperature dependence of resistivity is strongly suppressed with magnetic field. Upon applying magnetic field, the recovery of Fermi liquid behavior, $\rho \propto T^2$, is observed, independent of applied magnetic field directions at low temperatures (fig.S5a and b). The crossover temperature from non-Fermi liquid to Fermi liquid behavior, T_{FL} , is extracted from the deviation from T^2 -fit.

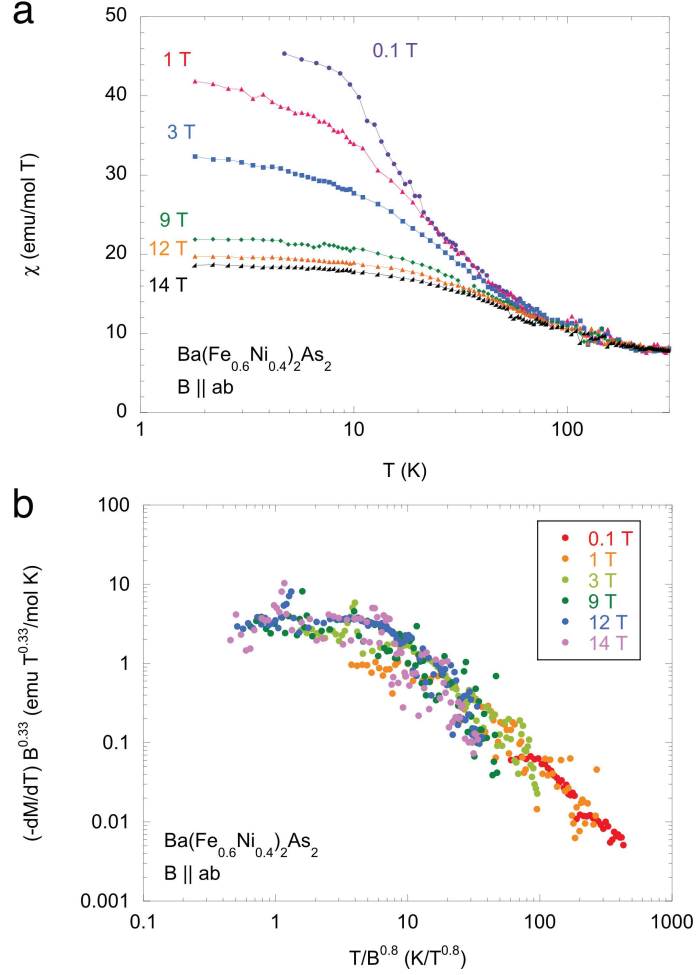


FIG. S4: **Quantum critical scaling in the magnetization for $\text{Ba}(\text{Fe},\text{Ni})_2\text{As}_2$.** **a**, Temperature dependence of the susceptibility χ for $\text{Ba}(\text{Fe},\text{Ni})_2\text{As}_2$ ($B \parallel ab$). Less diverging behavior in χ implies the system is located slightly far from the quantum critical point. **b**, Quantum critical scaling in the magnetization with critical exponents of $d/z = 2/3$ and $z\nu = 0.8$, slightly different from those extracted in $\text{Ba}(\text{Fe}_{1/3}\text{Co}_{1/3}\text{Ni}_{1/3})_2\text{As}_2$.

QUANTUM CRITICAL FERROMAGNETIC SCATTERINGS IN BaCo_2As_2

As evinced by the observation of the enhanced Wilson ratio and violation of the Korringa ratio, BaCo_2As_2 is located close to the ferromagnetic quantum instabilities. The instabilities actually cause unusual scatterings in the charge transport for BaCo_2As_2 (fig. S6a). Unlike $\text{Ba}(\text{Fe}_{1/3}\text{Co}_{1/3}\text{Ni}_{1/3})_2\text{As}_2$, the temperature dependence of resistivity for BaCo_2As_2 is not sublinear, but superlinear. To clarify the exponent of the temperature dependence, we plot the resistivity as a function of T^2 (fig. S6b), expected for Fermi liquid, and of $T^{5/3}$ (fig. S6c), expected for three dimensional quantum critical ferromagnets. Very similar to quantum critical ferromagnetic metal ZrZn_2 [2], the perfect linear-in- $T^{5/3}$ dependence of the resistivity below $T = 20$ K highlights the presence of abundant quantum critical scatterings in BaCo_2As_2 , robust against applied field, even up to 15 T.

ISOTROPY OF NON-FERMI LIQUID BEHAVIOR AND $\Gamma(T, B)$ SCALING

Despite of the quasi layered structure, the non-Fermi-liquid magnetoresistance of $\text{Ba}(\text{Fe}_{1/3}\text{Co}_{1/3}\text{Ni}_{1/3})_2\text{As}_2$ is independent of applied field orientations. Figure S6 shows the temperature dependence of resistivity in different applied field configurations. Independent of the applied field orientations, the quasi- T -linear dependence of resistivity at zero field is suppressed with field, suggesting the spatial dimensionality is three (fig. 1e in the main text).

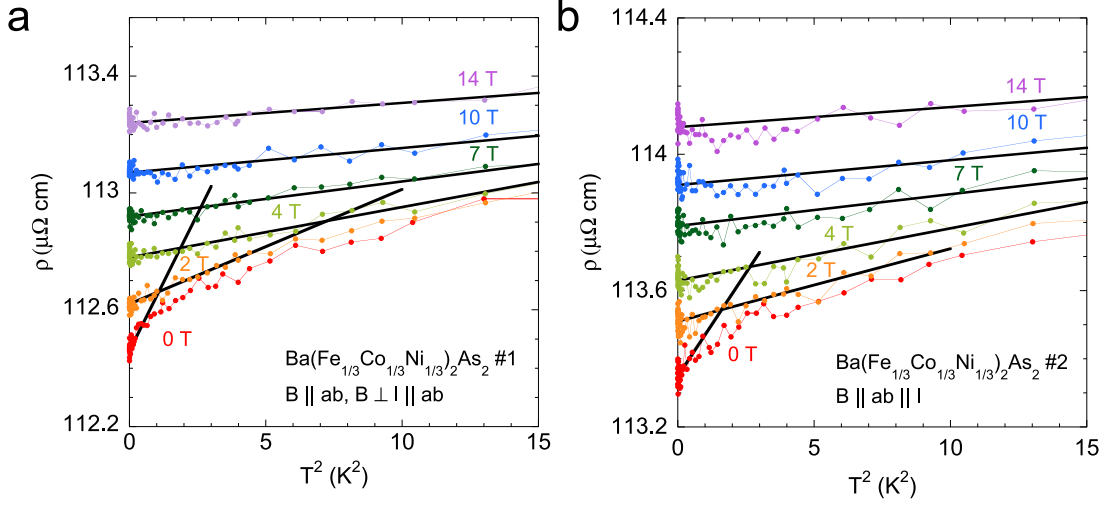


FIG. S5: **Non-Fermi liquid to Fermi liquid crossover in the resistivity for BaCo_2As_2 .** **a**, Resistivity as a function of T^2 for sample #1 in the configuration of $B \parallel ab, B \perp I \parallel ab$ and **b**, for sample #1 in the configuration of $B \parallel ab \parallel I$. Solid lines are linear fits to the data using $\rho = \rho_0 + AT^2$.

Obtaining from the magnetoresistance as shown in fig. S7, we plot $\Gamma(T, B)$ scaling in the resistivity, independent of field directions with respect to the current direction. For the in-plane field orientations ($B \parallel ab$), either longitudinal ($B \parallel I$) or transverse magnetoresistance ($B \perp I$) provides the ratio of scaling parameters of $\eta = 0.55$ (fig. S8a and b). By contrast, magnetoresistance in the perpendicular field orientation ($B \parallel c$) gives the ratio of $\eta = 0.67$ (fig. S8 c and d). The anisotropy of the scaling parameter ratio $\eta_{B \parallel ab} / \eta_{B \parallel c}$ is 0.82 and close to unity, suggesting isotropic scatterings. The non-Fermi liquid behavior in the magnetization measurements is also independent of applied field orientations, evidenced by the isotropy between the magnetization along $B \parallel c$ and $B \parallel ab$ (fig. S9).

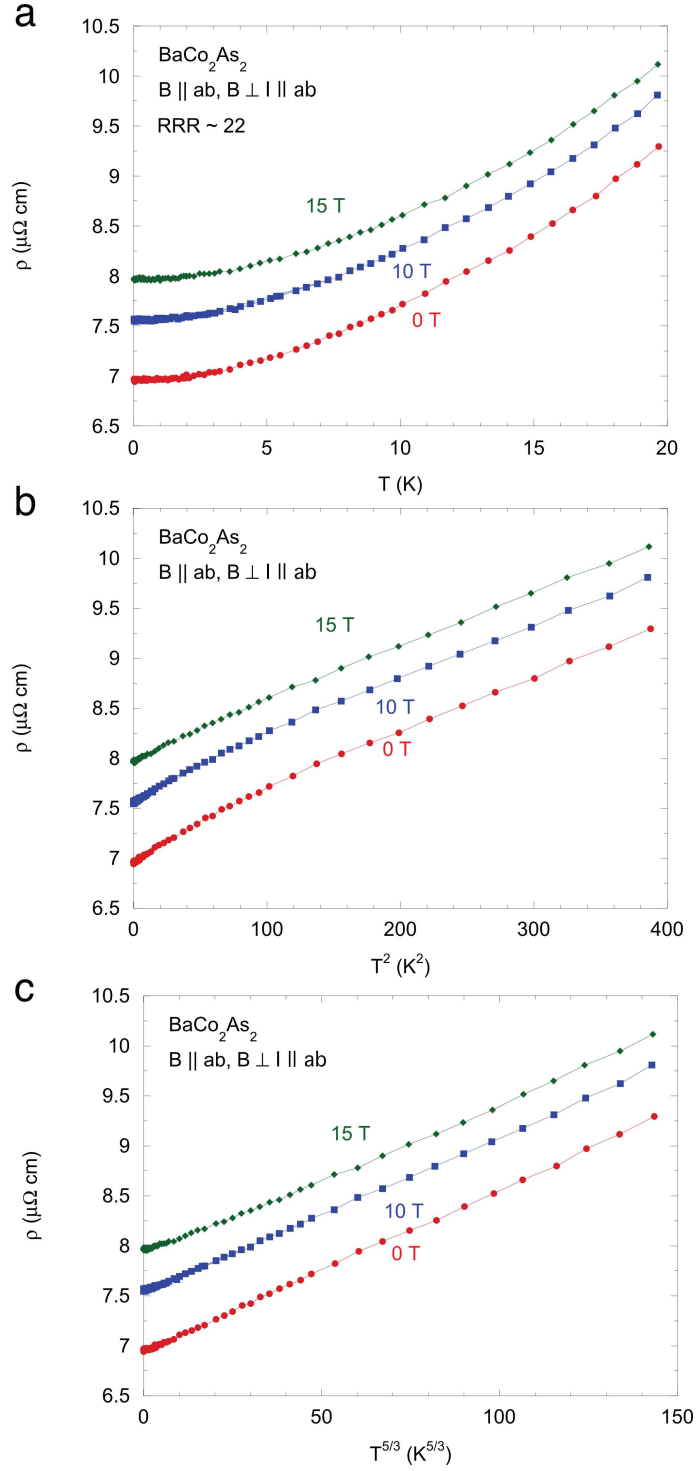


FIG. S6: **Ferromagnetic quantum critical scattering for BaCo_2As_2 .** **a**, Temperature dependence of resistivity for BaCo_2As_2 . The resistivity for BaCo_2As_2 as a function of **a**, T^2 and **b**, $T^{5/3}$, suggestive of ferromagnetic quantum critical scattering in 3D systems and reminiscent of marginal Fermi liquid ZrZn_2 .

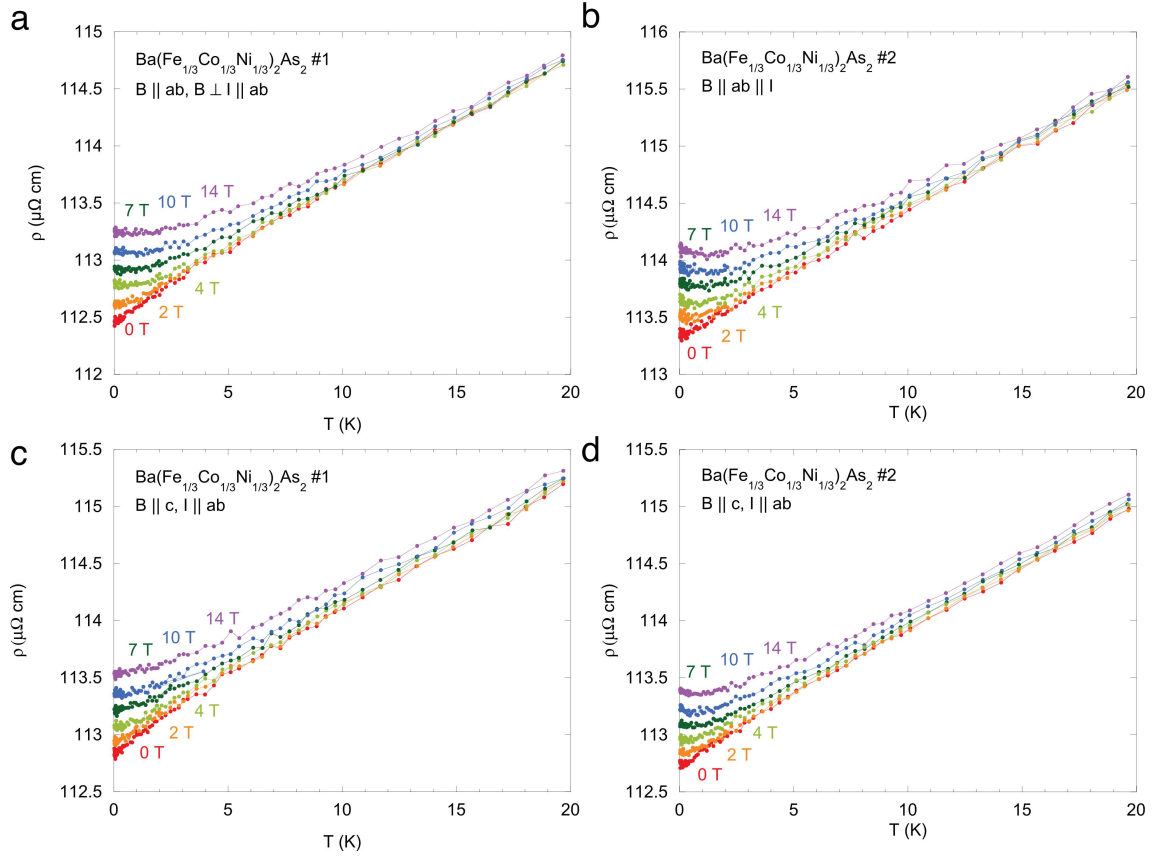


FIG. S7: **Isotropic magnetoresistance for $\text{Ba}(\text{Fe}_{1/3}\text{Co}_{1/3}\text{Ni}_{1/3})_2\text{As}_2$.** Resistivity as a function of T for **a**, sample #1 with $B \parallel ab$ and $B \perp I \parallel ab$, **b**, sample #2 with $B \parallel I \parallel ab$, **c**, sample #1 with $B \parallel c$ and $BI \parallel ab$, and **d**, sample #2 with $B \parallel c$ and $BI \parallel ab$.

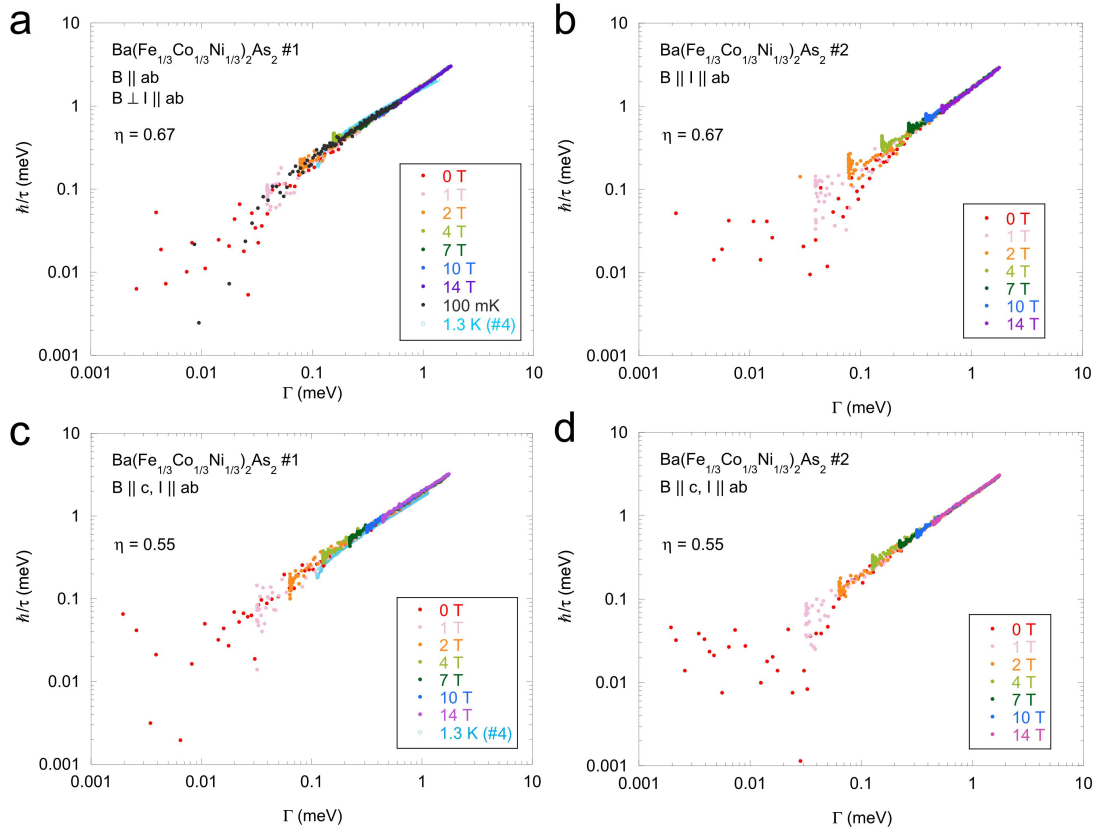


FIG. S8: **Anisotropy of $\Gamma(T,B)$ scaling for $\text{Ba}(\text{Fe}_{1/3}\text{Co}_{1/3}\text{Ni}_{1/3})_2\text{As}_2$ with different field orientations.** Resistivity as a function of $\Gamma \equiv \sqrt{(k_B T)^2 + (\eta \mu_B B)^2}$ for **a**, sample #1 with $B \parallel ab$ and $B \perp I \parallel ab$ together with sample #4 (scaled), **b**, sample #2 with $B \parallel I \parallel ab$, **c**, sample #1 together with sample #4 (scaled) and **d**, #2 with $B \parallel c$ and $I \parallel ab$.

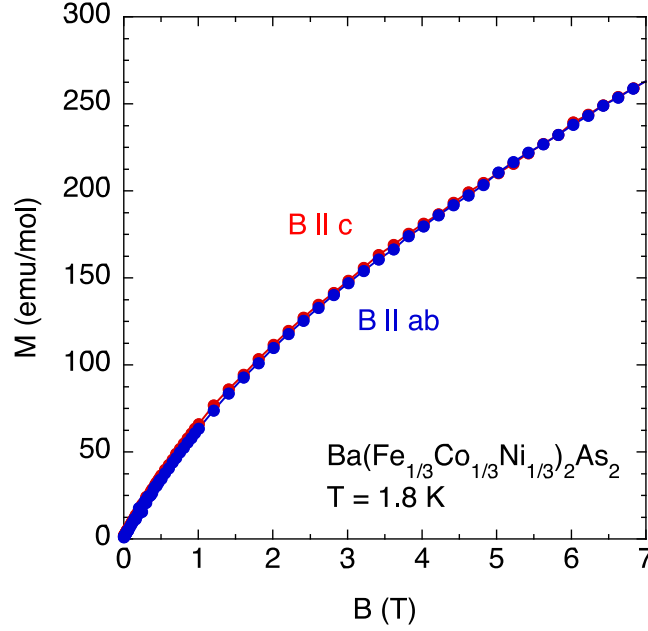


FIG. S9: **Isotropic magnetization for $\text{Ba}(\text{Fe},\text{Co},\text{Ni})_2\text{As}_2$.** Field dependence of magnetization along $B \parallel ab$ and $B \parallel c$ at $T = 1.8$ K. Despite of the layered structure, Anisotropy of magnetization is negligible, suggesting the system is three dimensional.

QUANTUM CRITICAL SCALING

The quantum critical scaling observed in magnetization (fig. 2c) and specific heat (fig. 2d) implies the presence of universal function of T/B in the free energy. We can assume the generic form for the free energy F as,

$$F(B, T) = T^{\frac{d+z}{z}} \tilde{f}_F \left(\frac{B}{T^{y_b/z}} \right) = B^{\frac{d+z}{y_b}} f_F \left(\frac{T}{B^{z/y_b}} \right), \quad (\text{S6})$$

where y_b is the scaling exponent related to magnetic field B , d is the spatial dimension, and z is the dynamical exponent. Assuming this form of free energy, we can derive magnetization $M = \partial F / \partial B$ and specific heat $C/T = -\partial^2 F / \partial T^2$. The magnetization is written by,

$$M = B^{(d+z)/y_b - 1} f_M \left(\frac{T}{B^{z/y_b}} \right), \quad (\text{S7})$$

where the scaling function f_M is also a universal function of $x = T/B^{z/y_b}$, given by,

$$f_M(x) = (d+z)/y_b f_F(x) - z/y_b f'_F(x). \quad (\text{S8})$$

To extract the critical exponents, we obtain the derivative of M ,

$$-\frac{dM}{dT} = B^{d/y_b - 1} f'_M \left(\frac{T}{B^{z/y_b}} \right). \quad (\text{S9})$$

By comparing this with the scaling relation observed in fig. 2c, the critical exponents yield,

$$\begin{cases} d/y_b - 1 = -1/3 \\ z/y_b = 1. \end{cases} \quad (\text{S10})$$

These equations provide

$$\begin{cases} z = y_b \\ d/z = 2/3. \end{cases} \quad (\text{S11})$$

Likewise, the specific heat can be given by,

$$\frac{C(B, T)}{T} = -\frac{\partial^2 F}{\partial T^2} = T^{(d-z)/z} \tilde{f}_C \left(\frac{B}{T^{y_b/z}} \right), \quad (\text{S12})$$

where $\tilde{f}_C(\tilde{x})$ is a scaling function of $\tilde{x} = B/T^{y_b/z}$,

$$\tilde{f}_C(\tilde{x}) = (d(d+z)/z^2) \tilde{f}_F(\tilde{x}) - (y_b(2d+z-y_b)/z^2) \tilde{x} \tilde{f}'_F(\tilde{x}) + (y_b^2/z^2) \tilde{x}^2 \tilde{f}''_F(\tilde{x}) \quad (\text{S13})$$

$$= (d(d+z)/z^2) \tilde{f}_F(0) + \tilde{g}_C(\tilde{x}), \quad (\text{S14})$$

where, $\tilde{g}_C(\tilde{x})$ is field-dependent part of $\tilde{f}_C(\tilde{x})$. Using this expression, we can extract field dependent part of specific heat,

$$\frac{\Delta C_e(B, T)}{T} = \frac{\Delta C_e(B, T)}{T} - \frac{\Delta C_e(0, T)}{T} = T^{\frac{d-z}{z}} \tilde{g}_C(B/T^{y_b/z}) = B^{\frac{d-z}{y_b}} g_C(T/B^{z/y_b}), \quad (\text{S15})$$

where $g_C(x)$ is temperature-dependent part of $f_C(x)$. By comparing this with the scaling relation in fig. 2d, we obtain the critical exponents yielding,

$$\begin{cases} (d-z)/y_b = -1/3 \\ z/y_b = 1, \end{cases} \quad (\text{S16})$$

also providing the same parameters as the eqs. (S6), namely,

$$\begin{cases} z = y_b \\ d/z = 2/3. \end{cases} \quad (\text{S17})$$

SCALING FUNCTION AND FERMI TO NON-FERMI LIQUID CROSSOVER

The obtained scaling relations clearly show the Fermi to non-Fermi liquid crossover behavior. For $T/B \gg 1$, we observe non-Fermi liquid diverging behavior in the susceptibility, $\chi \propto T^{-1/3}$, implying $f_M(x) \propto x^{-1/3}$. On the other hand, in the other limit of $T/B \ll 1$, we observed temperature independent susceptibility, suggestive of the recovery of FL regime. From these observations, we can write the asymptotic forms of $f_M(x)$,

$$f_M(x) \propto \begin{cases} x^{-1/3} & T \gg B \text{ quantum critical regime} \\ \text{const} + O(x^2) & T \ll B \text{ Fermi liquid regime.} \end{cases} \quad (\text{S18})$$

These asymptotic forms allow us to specify a universal function,

$$f_M(x) = c(x^2 + a^2)^{-1/6}, \quad (\text{S19})$$

reproducing the behavior in $x \ll 1$ and $x \gg 1$ limits. Using eq. (S6),

$$M = cB^{2/3}(x^2 + a^2)^{-1/6}. \quad (\text{S20})$$

The peak position in dM/dT gives the crossover temperature T^* by using $\frac{d}{dT}(dM/dT) = 0$, which gives,

$$T^*/B = x^* = \sqrt{3}a/2. \quad (\text{S21})$$

Extracted from this equation, $T^*(B)$ is plotted in the phase diagram (fig. 3c).

Similarly, T^* can also be extracted from the scaling in the specific heat, which follows the Maxwell relation linking the entropy to the magnetization,

$$\frac{\partial S(B, T)}{\partial B} = \frac{\partial M(B, T)}{\partial T}. \quad (\text{S22})$$

Integrating both sides with respect to B, we can obtain,

$$\int_0^B \frac{\partial S(B, T)}{\partial B} dB = \int_0^B \frac{\partial M(B, T)}{\partial T} dB. \quad (\text{S23})$$

Since

$$\int_0^B \frac{\partial S(B, T)}{\partial B} dB = S(B, T) - S(0, T) = \int_0^T \frac{\Delta C_e(B, T)}{T} dT, \quad (\text{S24})$$

using eq.(S6), (S18), and (S19), we get,

$$\frac{\Delta C_e(B, T)}{T} = \frac{\partial^2}{\partial T^2} \int_0^B M(B, T) dB = \int_0^B B^{-4/3} f_M''(x) dB, \quad (\text{S25})$$

where

$$f_M''(x) = -\frac{c}{3} (x^2 + a^2)^{-7/6} \left[1 - \frac{7}{3} \frac{x^2}{x^2 + a^2} \right]. \quad (\text{S26})$$

The peak positions in the scaling function of $\Delta C_e/T$ obtained from a fit to the data give the crossover temperature $T^*(B)$, consistent with T^* from M as plotted in the phase diagram (fig. 3c).

-
- [1] Kirshenbaum, K. *et al.* Tuning magnetism in FeAs-based materials via a tetrahedral structure. *Phys. Rev. B* **86**, 060504 (2012).
- [2] Sutherland, M. *et al.* Transport and thermodynamic evidence for a marginal Fermi-liquid state in ZrZn_2 . *Phys. Rev. B* **85**, 035118 (2012).